Scientia Iranica A (2021) 28(3), 1096–1108

Sharif University of Technology
Scientia Iranica
Transactions A: Civil Engineering
http://scientiairanica.sharif.edu

Evaluation of buckling load and dynamic performance of steel shear wall retrofitted with strips made of shape memory alloy

R. Kamgar[a], H. Heidarzadeh[a,*], and M.R. Babadaei Samani[b]

a. *Department of Civil Engineering, Faculty of Technology and Engineering, Shahrekord University, Shahrekord, P.O. Box 88186-34141, Iran.*
b. *Arian Saze Zagros Co., Chaharmahal Science & Technology Park, Shahrekord, Iran.*

Received 21 February 2019; received in revised form 5 October 2020; accepted 9 November 2020

KEYWORDS
Steel shear wall;
Shape-memory alloy;
Retrofitting;
Dynamic analysis;
Cyclic behavior;
Buckling analysis.

Abstract. The most common imperfections of a steel shear wall are out of plane displacements that cause severe damage in both structural and non-structural elements. In this paper, the effects of shape-memory alloys on steel shear walls are investigated. First, a numerical analysis, using the finite element method in Abaqus software, has been carried out according to an experimental test. The results of the numerical analysis have been verified with experimental results. Next, shape-memory alloy fibers have been added vertically and horizontally to various parts of the steel shear wall. The results show that retrofitting with the shape-memory alloy reduces the out-of-plane displacement of the steel shear wall under both cyclic and seismic loadings. Besides, the buckling load in the steel shear wall increases when it is retrofitted with the shape-memory alloy. Also, the total out-of-plane movement (accumulated absolute displacements) of the steel shear wall and non-structural damage are controlled by the characteristics of a shape-memory alloy material called "super-elastic".

1. Introduction

Steel Shear Walls (SSW) have been an efficient resistance system in structures against lateral loads [1–3]. This system can provide lateral stiffness and loading capacity in structures, especially in tall buildings [4]. The results of the studies show that SSW has appropriate resistance against severe earthquakes [5]. This system can also provide a large capacity for energy absorption, high deformation, and stable cyclic behavior; therefore, leading to the widespread use of SSW in various structures around the world. However, despite these abilities, if shear buckling occurs in a steel plate, the out-of-plane displacement of the plate reduces its ability in mild and moderate earthquakes [6].

Haddad et al. [7] studied several stiffened SSWs and showed that the shear stiffness, deformation capacity, and energy absorption increase by adding stiffeners to the steel plate. Shao et al. [8] proposed a new composite shear wall involving two steel plates and a concrete layer between them. Their analyses show that this new system has a considerable ability to provide high flexibility (deformation) and energy absorption in structures. Some experimental tests were performed on the performance of the ultra-thin-walled steel shear

*. *Corresponding author. Fax: +98 32324401*
E-mail address: heidarzadeh@sku.ac.ir (H. Heidarzadeh)

doi: 10.24200/sci.2020.52994.2991

wall by Chu et al. [9]. They found an increase in the resistance of the composite steel shear wall to the failure when a composite cold-framed is used. Besides, Liu et al. [10] studied steel shear wall performance when retrofitted by self-centering energy dissipation braces. They showed that good ductility and energy dissipation could be obtained for the proposed system subjected to cyclic loading. Tan et al. [11] also utilized hat-section cold-formed steel members to enhance steel shear wall resistance to buckling. They reported the design rules of the new proposed lateral bearing system. Besides, several investigations have been undertaken into the effects of applying other materials instead of steel in shear walls. De Matteis et al. [12] investigated the behavior of shear walls stiffened with aluminum. The experimental results exhibit that the energy absorption capacity of the shear wall increases because of the low yield stress of the aluminum material [12]. An investigation conducted by Shahi and Adibrad [13] on the low-yield-point steel shear wall behavior shows that the loading capacity of this kind of shear wall increases compared to ordinary SSW.

Besides, Ma et al. [6] designed an innovative buckling-restrained shear wall. In this system, low-yield-point steel is used as plate material, and lateral stiffeners are employed to prevent elementary buckling of the shear wall. The results reveal that plate buckling occurs in the higher levels, and therefore, the maximum drift ratio of the stories decreases.

In this paper, the dynamic behavior of SSW stiffened with Shape-Memory Alloy (SMA) is studied. Different methods can be used in static and dynamic analyses of structures [14–20]. One of the most powerful numerical time integration methods is the Newmark method, which can be used in the dynamic analysis of stiffened shear walls. Rahgozar et al. [21] used the Galerkin method to study the dynamic analysis of SSW. Besides, the effect of axial force on the mode shapes of shear walls has been studied by Rahgozar et al. [22]. An experimental investigation has been conducted to study the behavior of cold-formed SSW subjected to monotonic and cyclic loadings [23,24].

Based on the results obtained by the aforementioned studies, the out-of-plane displacement resulting from plate buckling significantly affects the SSW's performance. Therefore, in this paper, an innovative stiffened steel shear wall system is proposed. SMA strings are used in this system as stiffeners. Firstly, verification of the numerical simulation has been undertaken by modeling a steel frame of SSW in Abaqus software [25] and the results compared with an experimental test [26]. The same trend is then applied to verify the numerical method for an SMA bar based on experimental tests [27]. Next, the behavior of the stiffened SSW has been evaluated under both cyclic and seismic loadings; and the buckling capacity of the unstiffened and stiffened SSW is compared. The results show that the value of buckling load for stiffened SSW is increased. Also, out-of-plane deformation of the stiffened SSW is decreased.

2. Shape-Memory Alloy (SMA)

Nowadays, many investigations concentrate on structural retrofitting to increase load-carrying capacity, deformation, and energy absorption during dynamic loadings, and to reduce the damage values of structural and non-structural elements. Several studies have recently been undertaken on the behavior of SMA material [28].

SMA can return to its initial position after unloading, even after large deformations. This ability can be activated by heating and unloading, representing the "shape-memory" and "super-elastic" characteristics of this material. A schematic stress-strain curve of SMA material is shown in Figure 1. As shown in this figure, there is no residual deformation in SMA when unloading has been completed.

Besides, SMA has different mechanical characteristics than conventional steel; for example, the density and elastic modulus of Nickel-Titanium SMA are 6.45 g/cm^3 and 30–83 GPa, respectively. Also, Nickel-Titanium SMA can eliminate about 8% of residual strain during unloading [27].

Several studies have been implemented to identify SMA behavior. Andrawes and Shin [30] used SMA stirrups as the active confinement in the columns of concrete bridges. The results show that this material has a better effect on reducing the maximum drift of structures than Fiber-Resistant Polymer (FRP) laminates. This material can also be used to apply controlled pre-tension load to the structural elements [31]. Likewise, Izadi et al. [32] used iron-based SMA (Fe-SMA) to pre-stress the steel plate. This study has shown that the pre-stressing applied to steel plate

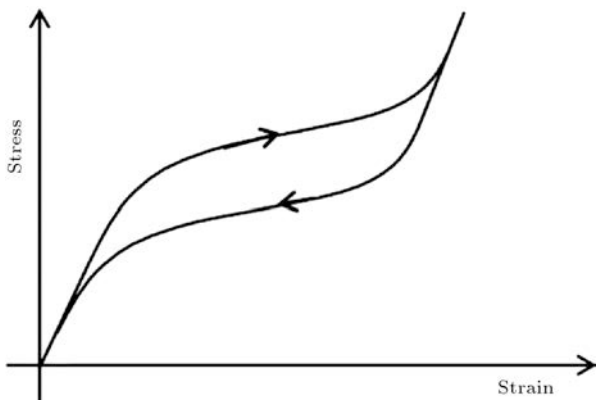

Figure 1. Stress-strain curve of Shape Memory Alloy (SMA) [29].

Table 1. Dimensions of the steel frame with Steel Shear Walls (SSW).

Element		Dimensions of section (mm)				Yield stress (MPa)	Ultimate stress (MPa)	Poison ratio	Modulus of elasticity (MPa)	Density (kg/m^3)
		h	b_f	t_w	t_f					
Beams	Str 1 & 2	200	200	16	16	330	600	0.3	2×10^5	7850
	Str 3	400	400	16	16					
Columns		250	250	20	20					

causes some increase in the steel plate's yield stress and fatigue resistance.

3. Verification of numerical analyses

3.1. Verification of numerical modeling of SSW

A one-bay, three-story steel frame with SSW presented by Park et al. [26] is selected and modeled using Abaqus software to verify the numerical analyses. The element dimensions of the steel frame and SSWs are shown in Table 1. Also, Figure 2 shows the parameters used in the definition of the sections. Finally, Figure 3 presents the stress-strain curve for the frame and SSW made of conventional steel materials, as listed in Table 1.

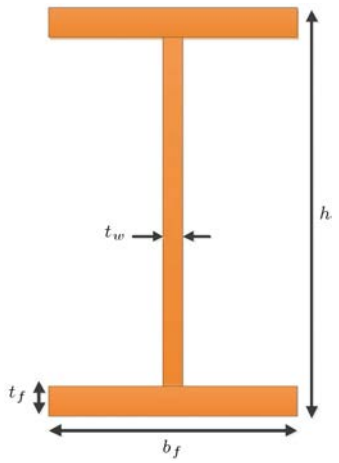

Figure 2. The parameters used in the definition of the beams and columns section.

In the numerical modeling by Abaqus, the C3D8R element type is used for beams and columns, and the S4R element type is employed for SSWs. It should be noted that the C3D8R element shows a three-dimensional linear brick element with eight nodes integrated with a reduced integration method (1 integration point). Besides, the S4R element presents a two-dimensional shell element that has four nodes. This type of element uses a reduced integration method with a large-strain formulation. The reduced integration method is used for all elements. Shear locking phenomena can occur for the first order, fully integrating elements (e.g., C3D8) subjected to the bending. The Abaqus benchmark manual states that using fully integrated standard displacement for 4-node shell and beam elements leads to a stiffer model (i.e., in-plane bending). Abaqus also proposes that using a reduced full integration method can lead to more accurate results when the number of elements is enough (several benchmarks have been presented for the beam structures by Abaqus). Therefore, to decrease the computational cost and running time, the reduced integration method is used based on the Abaqus recommendation, while the number of elements has been increased. The Abaqus user manual also points out that the running time reduces, especially for three-dimensional problems when the reduced integration method is used. Therefore, the running time and element assembly are decreased by using the C3D8R element. It also proposes using a full or reduced integration method for hexahedral (brick elements) in the Abaqus/Standard or Abaqus/Explicit. This user manual states that the reduced integration

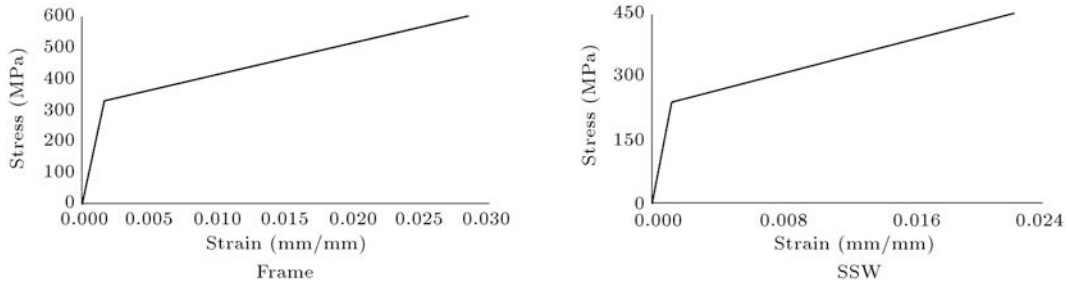

Figure 3. The stress-strain curve for the material used in the definition of the frame and Steel Shear Walls (SSW) made of conventionally steel materials.

method can calculate the structure's responses depending on the nature of the problem compared with the full integration method. There are three types of hardening (i.e., isotropic, kinematics, and combined). The combined hardening nested surface model involves a combination of isotropic and kinematic hardening rules. In the isotropic hardening rule, an expansion of the yield surface will occur when plastic strains are undergone. On the other hand, a shifting will also occur for the yield surface in the kinematic rule when plastic strain is experienced [33]. It should be noted that the kinematic-hardening model is used here to define a constant rate of cyclic hardening based on references [25,33]. For this purpose, the specifications of considered steels were selected from [26]. Also, since there were the results of a standard monotonic tension test, it is necessary to define the inelastic material properties by some assumption reported in [33]. For this purpose, characteristics of the cyclic loading materials are assumed to be equal to the monotonic loading based on the ATLSS report [33,34], as advised by Vian et al. [33]. Finally, the results show a good agreement between the numerical and experimental tests. It should be noted that the total number of used elements for the SSW was 1729, including 1279 C3D8 and 450 S4R. The thickness of the shear wall is 2 mm, and because the shell element was used for modeling of the steel shear wall, no mesh was used in the thickness direction. Besides, the size for all elements is the same and is equal to 100×100 mm for the S4R element. On the other hand, the minimum size of the mesh for the C3D8 element is 6.66 mm.

Also, cyclic loading has been applied on the top beam's left side as percentages of the structure yield displacement, as shown in Figure 4 [26]. It should be noted that this type of loading has been used to check the results obtained from the numerical model with those reported in [26] by an experimental test. The boundary conditions consist of fixed supports located at the end of the columns and bottom edge of the steel plate in the first story. Also, the lateral supports have been connected to both ends of the beams. This leads to avoiding out-of-plane displacement of the frame. The finite element mesh is exhibited in Figure 5.

A comparison between the results of the numerical and experimental data is illustrated in Figure 6. As shown in the load-displacement curve (Figure 6), the numerical results have an acceptable accuracy compared to the experimental data. The distribution pattern of out-of-plane displacement between the numerical and experimental results is presented in Figure 7. The numerical results have an acceptable accuracy in comparison with the experimental data

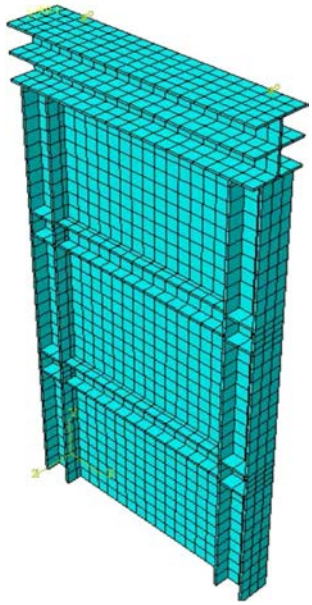

Figure 5. Finite element mesh generated for the steel frame.

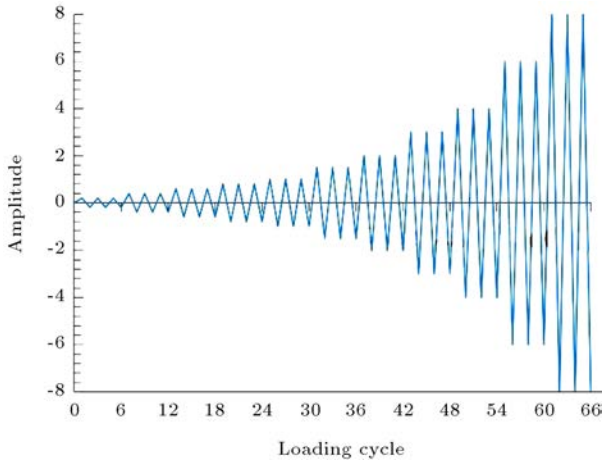

Figure 4. The amplitude pattern used in the cyclic loading [26].

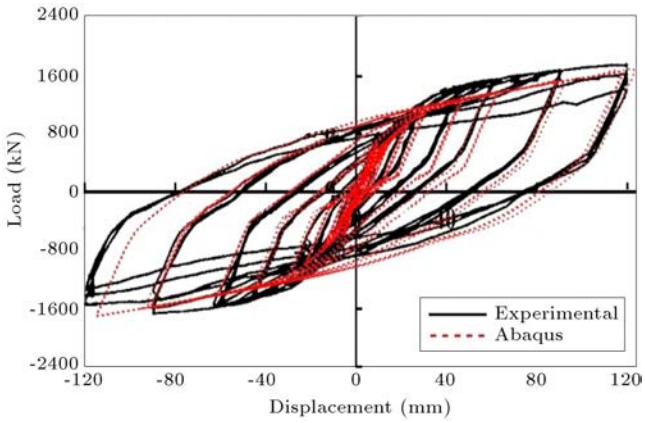

Figure 6. The load-displacement curve of the steel frame retrofitted with Steel Shear Walls (SSW) subjected to the cyclic loading.

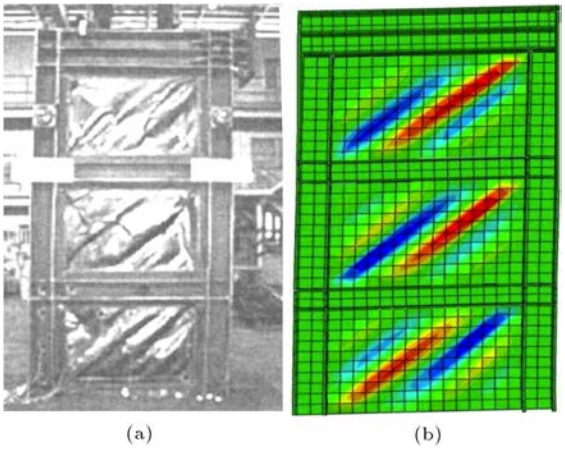

Figure 7. Ultimate deformation of the steel frame with Steel Shear Walls (SSW) under cyclic loading: (a) Experimental observations [26] and (b) numerical analysis.

based on these figures. Therefore, it could be concluded that the Abaqus model can be used for future studies.

3.2. Verification for numerical modeling of SMA material

Two experimental tests were also carried out on an SMA bar under cyclic loading [27,35]. The bar is modeled in Abaqus software using super elasticity material. The diameter of the bar is 25.4 mm and has been made of Nickel-Titanium SMA. Cyclic loading is applied to the free end of the bar, and the other end is fixed in all directions. The values of the parameters used in the numerical analysis are shown in Table 2. Also, the stress-strain relation of these materials is shown in Figure 8.

Comparisons between the results of the numerical and experimental analyses are shown in Figure 9. As shown in Figure 9, there is good agreement between the numerical results and experimental data; hence, the numerical modeling has an appropriate ability to predict the behavior of the SMA material.

4. SSW retrofitted with SMA

In this section, the one-bay three-story frame is considered, and the SSW are retrofitted with SMA strips made of material 1. The SMA strips are placed in both vertical and horizontal directions in the middle area of the plate (see Figure 10). The effects of retrofitting SSW with SMA are investigated in three phases: cyclic behavior, seismic behavior, and buckling analysis. The dimensions of SMA strips are shown in Figure 10. It should be noted that the total number of used elements

Table 2. The properties of Shape Memory Alloy (SMA) material.

SMA type	Parameter	Definition	Value
Material 1	E	Elasticity modulus	28 GPa
	υ	Poisson ratio	0.3
	sig_AM_s	Austenite to martensite starting stress	330 MPa
	sig_AM_f	Austenite to martensite finishing stress	580 MPa
	sig_MA_s	Martensite to austenite starting stress	300 MPa
	sig_MA_f	Martensite to austenite finishing stress	150 MPa
Material 2	E	Elasticity modulus	
	υ	Poisson ratio	
	sig_AM_s	Austenite to martensite starting stress	350 MPa
	sig_AM_f	Austenite to martensite finishing stress	600 MPa
	sig_MA_s	Martensite to austenite starting stress	200 MPa
	sig_MA_f	Martensite to austenite finishing stress	40 MPa

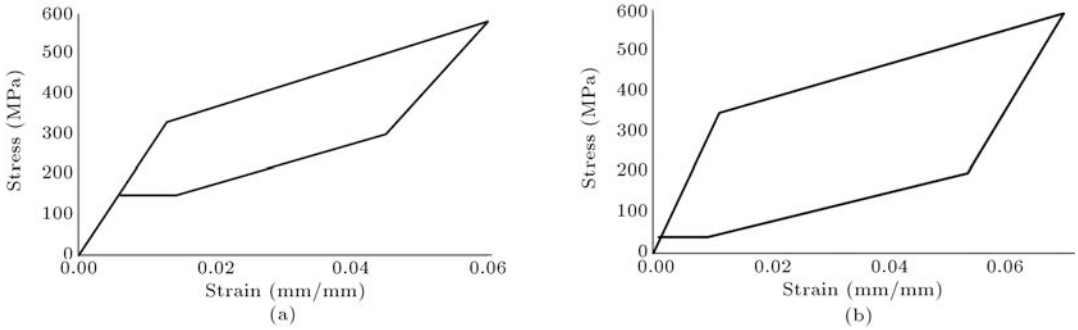

Figure 8. The stress-strain relation of the Shape Memory Alloy (SMA) material used in this study: (a) Material 1 [27] and (b) material 2 [35].

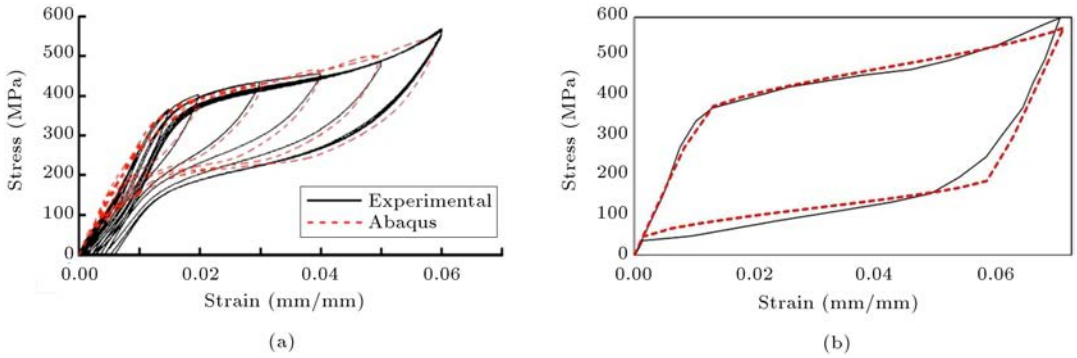

Figure 9. The load-displacement curve of the Shape Memory Alloy (SMA) bar subjected to the cyclic loading: (a) Material 1 [27], and (b) material 2 [35].

for the mentioned structure was 3457, including 1279 C3D8 and 2178 S4R. The thickness of the shear wall is 2 mm, and because the shell element was used for modeling of the steel shear wall, no mesh was used in the thickness direction. Besides, all elements in the steel shear wall are the same and equal to 100×100 mm. This size is 50 × 50 mm for the SMA strips. On the other hand, the minimum size of the mesh for the C3D8 element is 6.66 mm. It should be noted that contact between the SMA strips and the steel shear wall was considered to be hard. Also, friction has not been modeled here. In this regard, the SMA strips are considered as slave parts with smaller mesh. Also, the steel shear wall is assumed to be a master part with larger mesh. The connections between the steel plate and SMA strips have been made using laser welding.

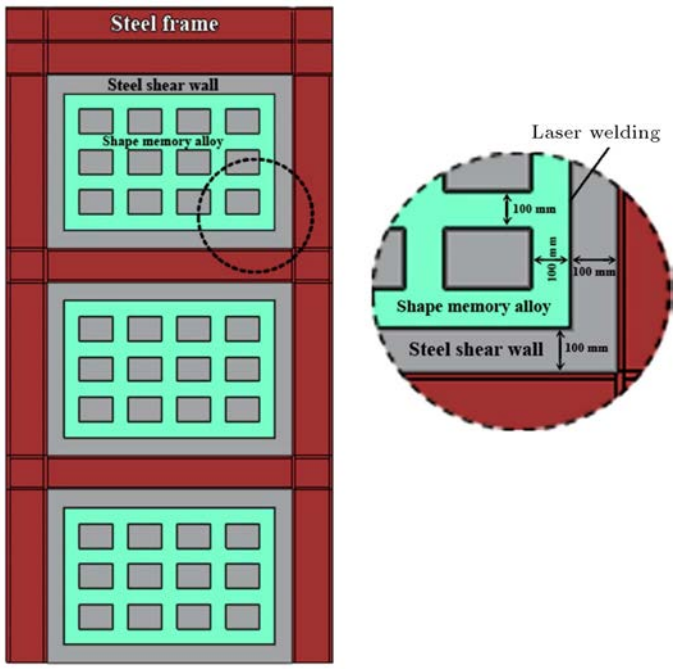

Figure 10. The steel frame retrofitted with Steel Shear Walls (SSW) and Shape Memory Alloy (SMA) strips.

This type of weld has been proposed by Oliveria et al. [36] for SMA materials.

4.1. Evaluation of the cyclic behavior of the SSW retrofitted with SMA

The mentioned cyclic loading is applied to the SSW and SSW retrofitted with SMA to evaluate the effects of SMA strips on the SSW's cyclic behavior. The absolute values of out-of-plane displacement and average values of stress in the SSW and SSW retrofitted with SMA and subjected to cyclic loading are exhibited in Figures 11 and 12, respectively. Besides, the envelope curve of these quantities has been shown in Figures 11 and 12. Based on Figures 11 and 12, the results are extracted with 66 cycles and implemented in Table 3.

As shown in Figures 11 and 12, this configuration of SMA strips decreases the value of out-of-plane displacement and the average value of stress for the steel plate, in almost all cyclic loading. The reduction percentages of the out-of-plane displacement and average stress value are 31% and 19%, respectively. It should be noted that the out-of-plane displacement and stress values of the SSW have been decreased

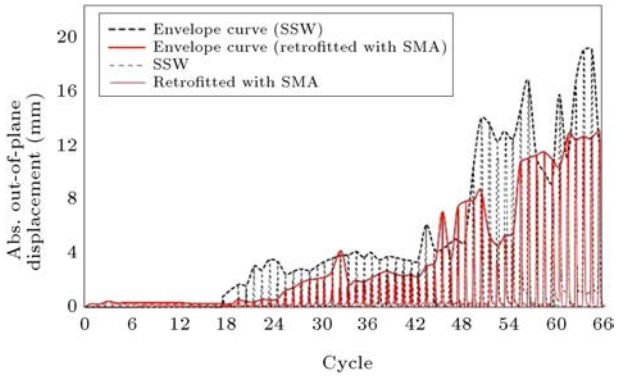

Figure 11. Absolute values of out-of-plane displacement in Steel Shear Walls (SSW) and SSW retrofitted with Shape Memory Alloy (SMA) subjected to the cyclic loading.

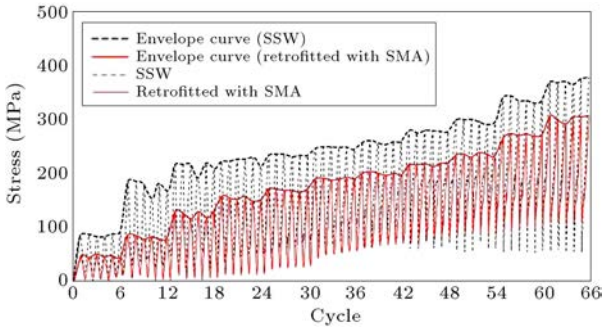

Figure 12. Average stress values in the Steel Shear Walls (SSW) and SSW retrofitted with Shape Memory Alloy (SMA) subjected to the cyclic loading.

Table 3. Summary results of the cyclic analyses obtained from 66 cycles.

Model	Abs. value of out-of-plane disp. (mm)	The average value of stress (MPa)
SSW	19.17	381.19
Retrofitted with SMA	13.19	307.73
Reduction percentage	31%	19%

by the super-elastic characteristics of the SMA material.

4.2. Seismic behavior evaluation of the retrofitted SSW with SMA

Based on the cyclic loading results, it could be deduced both the out-of-plane displacement and stresses decrease in the SSW retrofitted with SMA. Therefore, it seems that retrofitting with SMA can improve the behavior of SSW under dynamic loadings. In this section, the seismic behavior of the retrofitted SSW with SMA is investigated. For this purpose, four earthquake records have been selected and scaled with the Peak Ground Acceleration (PGA) value of the Gazli earthquake. Table 4 and Figure 13 show the characteristics and time history acceleration of the scaled earthquakes. These earthquakes are selected so that they cover three different categories of the Chandler classifications.

According to Chandler's classification [37,38], the accelerograms are divided into three sets based on their (PGA/PGV) ratios, in which PGA and Peak Ground Velocity (PGV) show the PGA and velocity of the earthquake, respectively [37]. The (PGA/PGV) ratios of the four different earthquakes adopted in this paper are given in Table 4.

Dynamic analyses have been performed for the intended earthquakes. For this purpose, the Newmark method [17] has been used to solve the equations of motion subjected to earthquake loads (see Eq. (1)):

$$[M]\{\ddot{u}\} + [C]\{\dot{u}\} + [K]\{u\} = -[M]\{\iota\}\ddot{u}_g, \tag{1}$$

where $[M]$, $[C]$, $[K]$, $\{u\}$, $\{\dot{u}\}$, $\{\ddot{u}\}$, and $\{\iota\}$ show the mass matrix, damping matrix, stiffness matrix, displacement vector, velocity vector, acceleration vector, and influence vector, respectively [17]. $\ddot{u}_g$ represents the acceleration of the ground motion.

The Loma Prieta, Landers, and Gazli are real time earthquakes, while the artificial earthquake is calculated based on [39] using the Gaussian white noise process and based on the Kanai-Tajimi filter and Power Spectral Density Function (PSDF), as follows [39–41]:

$$S_{\text{Kanai-Tajimi}}(\omega) = S_0\left[\frac{\omega_g^4 + (2\times\omega_g\times\xi_g\times\omega)^2}{(\omega^2-\omega_g^2)^2+(2\times\omega_g\times\xi_g\times\omega)^2}\right],$$

$$S_0 = \frac{0.03\times\xi_g}{\pi\times\omega_g\times(4\times\xi_g^2+1)}, \tag{2}$$

where S_0, ω_g, and ξ_g are the intensity of the soil PSDF, frequency, and damping, respectively. The values of ω_g and ξ_g are considered to be equal to 25.13 (rad/sec) and 0.8, respectively, based on Wu et al. [42]. This indicates that the structure has been located on stiff soil.

The results of the seismic analyses are shown in Figure 14 and Table 5. According to these results, retrofitting with SMA decreases the maximum out-of-plane displacement of SSW subjected to all the intended earthquakes, especially in the duration of strong ground motion (these times are specified with two vertical lines in Figure 14). The reduction percentages of the maximum out-of-plane displacement for Loma Prieta, Landers, Gazli, and artificial earthquakes are 12.73, 1.0, 44.43, and 16.96, respectively. It should

Table 4. Characteristics of the scaled earthquakes.

Earthquake	PGA (g)	PGV (m/sec)	PGA/PGV (g.sec/m)	Strong ground motion duration (sec)	Total time duration (sec)	Arias intensity (m/sec)
Loma Prieta	0.8639	0.765	**1.129**	9.815	25.0	15.674
Landers	0.8639	0.841	**1.027**	10.577	27.998	11.362
Gazli	0.8639	0.676	**1.277**	6.956	13.0878	5.672
Artificial	0.8639	1.540	**0.561**	17.760	20	22.492

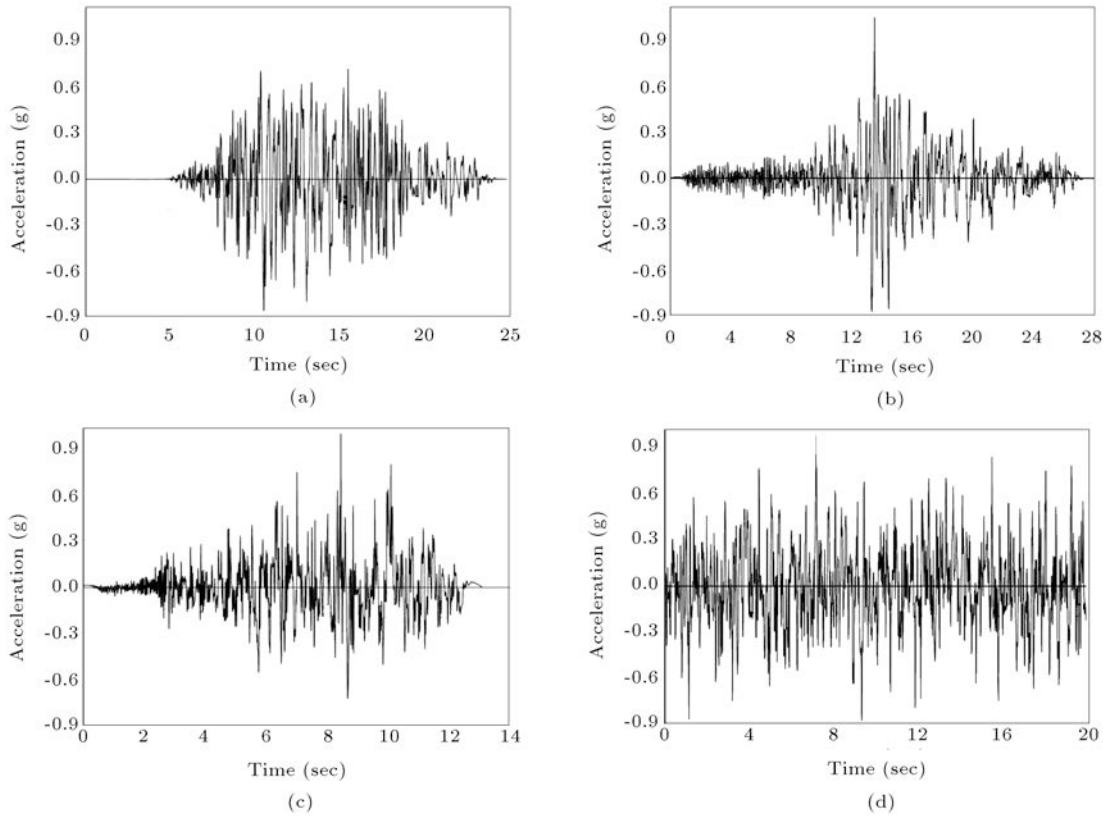

Figure 13. Time history acceleration of the scaled earthquakes: (a) Loma Prieta, (b) Landers, (c) Gazli, and (d) artificial.

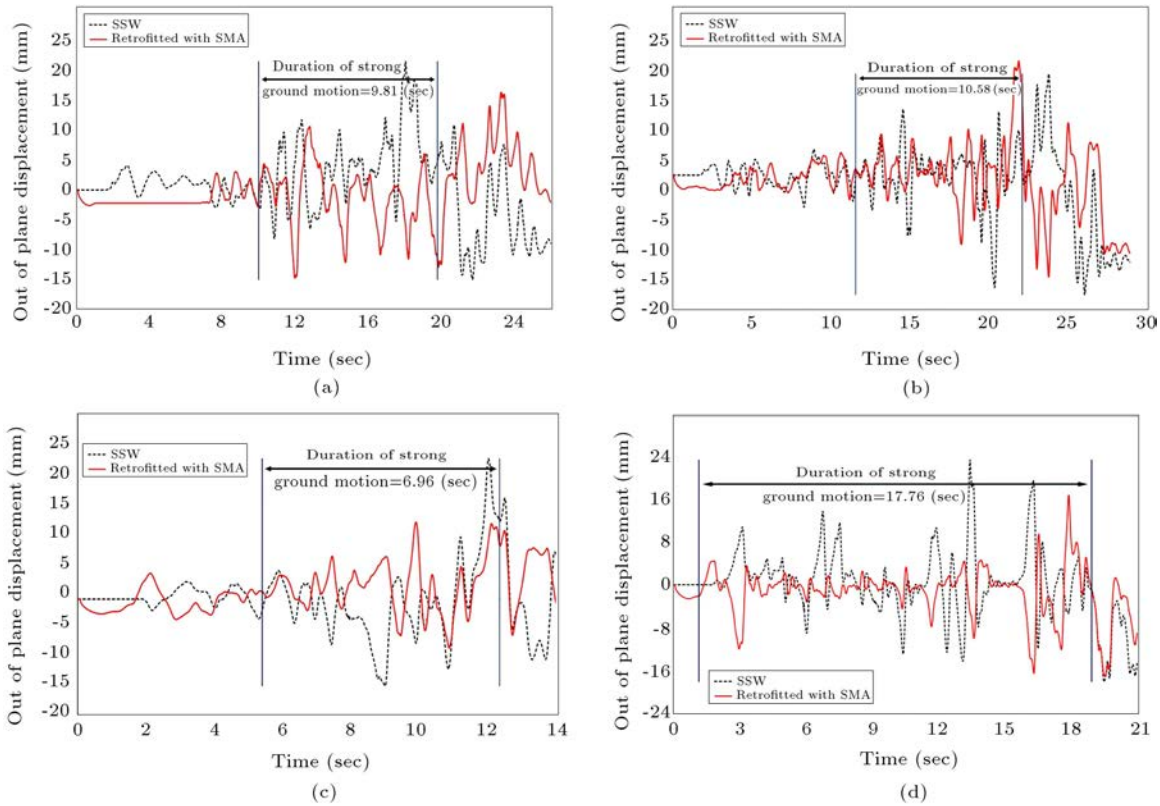

Figure 14. The average values of out-of-plane displacement of the Steel Shear Walls (SSW) subjected to the earthquakes: (a) Loma Prieta, (b) Landers, (c) Gazli, and (d) artificial.

Table 5. The reduction percentage of the out-of-plane displacement in the Steel Shear Walls (SSW) retrofitted with Shape Memory Alloy (SMA).

Earthquake	The maximum value of out-of-plane disp.	Total value for out-of-plane movement in shear wall
	Reduction percentage due to retrofitting with SMA	
Loma Prieta	12.73%	23.41%
Landers	1.0%	12.94%
Gazli	**44.43%**	15.26%
Artificial	16.96%	**31.64%**

be noted that these values are computed in all nodes of used mesh for the SSW retrofitted with SMA for maximum values over the whole time duration. It can be noted that Gazli is a near-field earthquake, and the maximum effect in the reduction of the maximum out-of-plane displacement occurs when subjected to this earthquake. Also, retrofitting with SMA changes the phase of out-of-plane displacement in the steel plate. It also reduces the total out-of-plane movements (accumulated absolute displacements over the whole time duration). The reduction value of the total out-of-plane movement occurs when subjected to the artificial earthquake by 31.64%.

Figure 15 and Table 6 show a comparison between the values of the average stresses occurred in the SSW when subjected to the intended earthquakes. The results are almost the same as the obtained results during cyclic loading. It should be noted that SMA and steel materials have almost the same yield and ultimate stresses; hence, no significant change is expected in the maximum values of the stresses in the SSW retrofitted with SMA when compared with the SSW. The "super-elastic" characteristics of SMA materials lead to these valuable differences between SSW and SSW retrofitted with SMA.

Table 6. The reduction percentage of the maximum stress value in the Steel Shear Walls (SSW) retrofitted with Shape Memory Alloy (SMA).

Earthquake	Percent reduction of maximum stress value
Loma Prieta	**−1.89%**
Landers	4.30%
Gazli	1.16%
Artificial	**5.39%**

The von Mises stress contours for the shear wall at

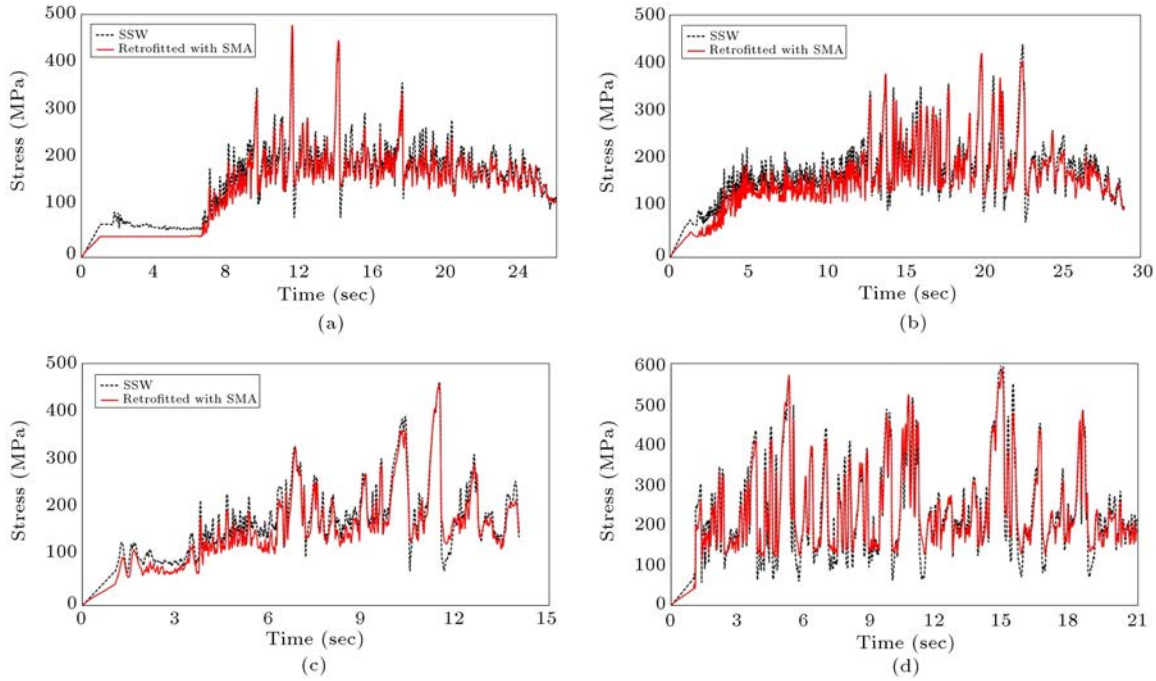

Figure 15. The average values of stresses in the Steel Shear Walls (SSW) and SSW retrofitted with Shape Memory Alloy (SMA) subjected to the earthquakes: (a) Loma Prieta, (b) Landers, (c) Gazli, and (d) artificial.

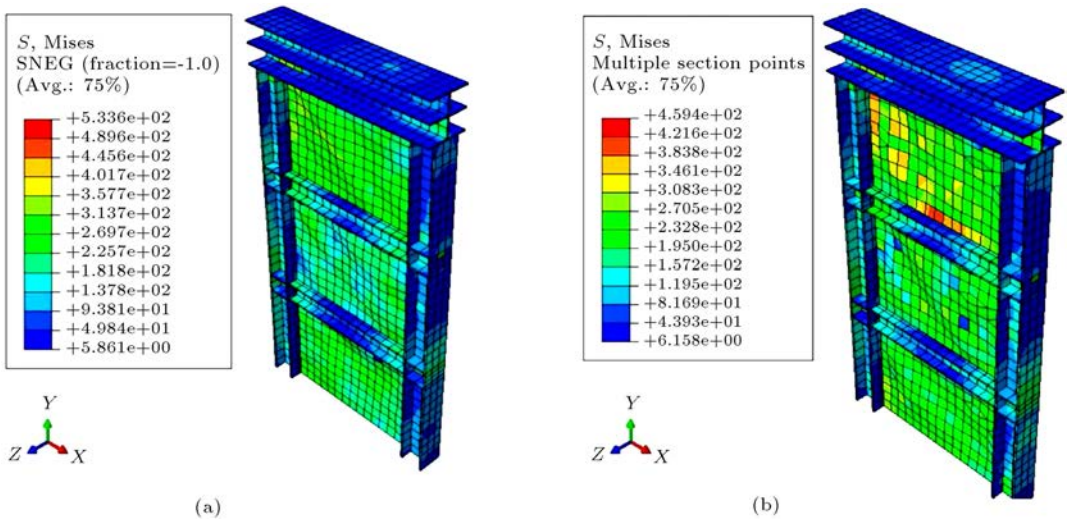

Figure 16. Contours of the von Mises stress for the shear walls at the end of the dynamic analyses: (a) Steel Shear Walls (SSW) subjected to the artificial earthquake and (b) SSW retrofitted by Shape Memory Alloy (SMA) strips subjected to the artificial earthquake.

the termination time instance of the dynamic analyses have been provided in Figure 16.

Commonly, in explicit Abaqus with a different definition of materials and suitable support conditions following the experimental program, different failure modes such as yield, rupture, buckling, and so forth, can occur and be modeled. In this model, according to experimental results, the main failure was in the form of shear wall buckling, shown in Figure 7. Also, in the present studies, the yield mechanism has been well demonstrated by adding SMA strips to the steel shear wall, as presented in Figure 16.

4.3. Evaluation of the buckling analysis in the SSW retrofitted with SMA

The main reason for the out-of-plane displacement in SSW is the buckling occurred in the steel plate. Moreover, the local buckling of the steel plate reduces the lateral loading capacity. In this section, the effect of retrofitting with SMA on the SSW buckling load capacity is investigated. Several numerical analyses have been implemented in Abaqus software, and the results of three modes are shown in Table 7.

As shown in Table 7, SMA increases the structure's buckling load capacity by more than 50%. Therefore, this effect can decrease the damage of the structural and non-structural elements.

Table 7. The comparison between the buckling loads capacity (kN).

Mode	Steel frame with SSW	Steel frame with SSW retrofitted with SMA	Increased percentage of buckling load
1	19.07	38.80	50.85%
2	20.80	42.04	50.52%
3	21.45	42.91	50.01%

5. Conclusion

The main purpose of this paper is to study the behavior of the Steel Shear Walls (SSW) retrofitted with Steel Memory Alloy (SMA) strips. Toward this aim, firstly, a steel structure with SSW and an SMA bar have been modeled in Abaqus software. Then, validation of the numerical analyses has been fully implemented by comparison with some experimental results. Next, several numerical models have been investigated in the case of cyclic and seismic loadings, and also buckling analysis. Briefly, the following results have been extracted:

1. SMA strips reduce the values of the out-of-plane displacement of SSWs under cyclic loading by 31%. Also, the average stress of SSWs decreases by 19% due to retrofitting SSW with SMA. Therefore, SMA strips can decrease the steel plates displacement and stress values because of their unique super-elastic characteristics;
2. The same results, as discussed in case 1, have been deduced for seismic analyses of SSW retrofitted with SMA. The reduction in the out-of-plane displacement of SSW has been clearly exhibited in the structure's analyses under various earthquakes, especially during strong ground motion. Hence, SMA could well confine the out-of-plane displacement of SSW. It should be noted that the maximum effect on confinement occurred under the Gazli earthquake, which is a near field earthquake;

3. Retrofitting SSW with SMA changes the phase of the out-of-plane displacement of SSW and decreases the total out-of-plane movement of the steel plate. In other words, SMA limits the out-of-plane vibrations of SSW;
4. Although SMA and steel materials have almost the same yield and ultimate stresses, no significant effect is expected on the stress of SSW and retrofitting the SSW with SMA. The "superelastic" characteristics of SMA material leads to these valuable differences between the SSW and SSW retrofitted with SMA. The average value of stress in the SSW has been almost reduced under seismic analyses. Hence, this effect can decrease the tearing of the steel plate;
5. The results of buckling analyses show that SMA retrofitting will lead to an increase in the values of buckling load for the first three natural modes of the steel frame with SSW by more than 50%. The main reason for the increase in the buckling loads of the SSW retrofitted with SMA is inversely related to the out-of-plane displacement. Besides, a decrease in the out-of-plane displacement will increase the buckling load capacity due to good confinement induced by SMA strips;
6. SMA strips, due to their unique characteristics, can well limit structural and non-structural damage under earthquakes, according to the reduction observed in the out-of-plane displacement. Also, they can postpone the failure of the SSW. Therefore, this can be a good retrofitting method to strengthen existing steel structures against earthquake load.

Acknowledgment

The authors greatly appreciate the support of the HPC center (Shahr-e-Kord University, Iran) for their collaboration in offering computational clusters, which was of great assistance in the completion of this work.

References

1. Akbarzadeh Bengar, H., Mohammadalipour, A., and Ski, R. "Effect of steel and concrete coupling beam on seismic behavior of rc frame accompanied with coupled shear walls", *Scientia Iranica*, **24**(5), pp. 2227–2241 (2017).
2. Emami, F. and Mofid, M. "On the improvement of steel plate shear wall behavior, using energy absorbent element", *Scientia Iranica*, **24**(1), pp. 11–18 (2017).
3. Kamgar, R., Askari Dolatabad, Y., and Babadaei Samani, M.R. "Seismic optimization of steel shear wall using shape memory alloy", *International Journal of Optimization in Civil Engineering*, **9**(4), pp. 671–687 (2019).
4. Wang, M. and Yang, W. "Hysteretic behaviors study of thin steel plate shear wall structures", *Journal of Building Structures*, **36**(1), pp. 68–77 (2015).
5. Ge, M., Hao, J., Yu, J., Yan, P., and Xu, S. "Shaking table test of buckling-restrained steel plate shear walls", *Journal of Constructional Steel Research*, **137**, pp. 254–261 (2017).
6. Ma, Z.-y., Hao, J.-p., and Yu, H.-s. "Shaking-table test of a novel buckling-restrained multi-stiffened low-yield-point steel plate shear wall", *Journal of Constructional Steel Research*, **145**, pp. 128–136 (2018).
7. Haddad, O., Sulong, N., and Ibrahim, Z. "Cyclic performance of stiffened steel plate shear walls with various configurations of stiffeners", *Journal of Vibroengineering*, **20**(1), pp. 459–476 (2018).
8. Shao, J.-h., Gu, Q., and Shen, Y.-k. "Seismic performance evaluation of steel frame-steel plate shear walls system based on the capacity spectrum method", *Journal of Zhejiang University-SCIENCE A*, **9**(3), pp. 322–329 (2008).
9. Chu, Y., Hou, H., and Yao, Y. "Experimental study on shear performance of composite cold-formed ultra-thin-walled steel shear wall", *Journal of Constructional Steel Research*, **172**, p. 106168 (2020).
10. Liu, J., Xu, L., and Li, Z. "Development and experimental validation of a steel plate shear wall with self-centering energy dissipation braces", *Thin-Walled Structures*, **148**, p. 106598 (2020).
11. Tan, J.-K., Gu, C.-W., Su, M.-N., Wang, Y.-H., Wang, K., Shi, Y., Lan, Y.-S., Luo, W., Deng, X.-W., Bai, Y.-T., and Chen, Q. "Finite element modelling and design of steel plate shear wall buckling-restrained by hat-section cold-formed steel members", *Journal of Constructional Steel Research*, **174**, p. 106274 (2020).
12. De Matteis, G., Mazzolani, F., and Panico, S. "Experimental tests on pure aluminium shear panels with welded stiffeners", *Engineering Structures*, **30**(6), pp. 1734–1744 (2008).
13. Shahi, N. and Adibrad, M.H. "Finite-element analysis of steel shear walls with low-yield-point steel web plates", *Proceedings of the Institution of Civil Engineers-Structures and Buildings*, **171**(4), pp. 326–337 (2017).
14. Fadaee, M., Saffari, H., and Khosravi, H. "Mathematical approach for large deformation analysis of the stiffened coupled shear walls", *International Journal of Applied Science, Engineering Technology*, **2**(5), pp. 110–113 (2008).
15. Saffari, H., Abbasnia, R., and Amini, F. "Extended slope-deflection method for nonlinear analysis of thin walled structures (in Persian)", *International Journal of Science & Technology*, **1**, pp. 79–102 (2000).

16. Fadaee, M.J., Saffari, H., and Khosravi, H. "Stability of stiffened coupled shear-wall", *Journal of Tehran School of Engineering*, **4**(4), pp. 667–676 (2006).

17. Kamgar, R. and Rahgozar, R. "A simple method for determining the response of linear dynamic systems", *Asian Journal of Civil Engineering*, **17**(6), pp. 785–801 (2016).

18. Rostami, S. and Shojaee, S. "Alpha-modification of cubic B-Spline direct time integration method", *International Journal of Structural Stability and Dynamics*, **17**(10), p. 1750118 (2017).

19. Rostami, S. and Shojaee, S. "A family of cubic B-spline direct integration algorithms with controllable numerical dissipation and dispersion for structural dynamics", *Iranian Journal of Science and Technology, Transactions of Civil Engineering*, **42**(1), pp. 17–32 (2018).

20. Sivandi-Pour, A., Gerami, M., and Kheyroddin, A. "Uniform damping ratio for non-classically damped hybrid steel concrete structures", *International Journal of Civil Engineering*, **14**(1), pp. 1–11 (2016).

21. Rahgozar, R., Mahmoudzadeh, Z., Malekinejad, M., and Rahgozar, P. "Dynamic analysis of combined system of framed tube and shear walls by Galerkin method using B-spline functions", *The Structural Design of Tall and Special Buildings*, **24**(8), pp. 591–606 (2015).

22. Rahgozar, R., Malekinejad, M., and Jahanshahi, M. R. "Free vibration analysis of coupled shear walls with axial force effects", *The IES Journal Part A: Civil and Structural Engineering*, **4**(4), pp. 224–231 (2011).

23. Wang, J., Wang, W., Xiao, Y., and Yu, B. "Cyclic test and numerical analytical assessment of cold-formed thin-walled steel shear walls using tube truss", *Thin-Walled Structures*, **134**, pp. 442–459 (2019).

24. Xie, Z., Yan, W., Yu, C., Mu, T., and Song, L. "Experimental investigation of cold-formed steel shear walls with self-piercing riveted connections", *Thin-Walled Structures*, **131**, pp. 1–15 (2018).

25. ABAQUS, C., *Analysis User's Manual, Version 6.12*, *ABAQUS* (2012).

26. Park, H.-G., Kwack, J.-H., Jeon, S.-W., Kim, W.-K., and Choi, I.-R. "Framed steel plate wall behavior under cyclic lateral loading", *Journal of Structural Engineering*, **133**(3), pp. 378–388 (2007).

27. DesRoches, R., McCormick, J., and Delemont, M. "Cyclic properties of super elastic shape memory alloy wires and bars", *Journal of Structural Engineering*, **130**(1), pp. 38–46 (2004).

28. Arvin, A. and Read, J. "Internal and external reinforcement of concrete members by use of shape memory alloy and fiber reinforced polymers under cyclic loading: A review", *Polymers*, **10**(4), p. 376 (2018).

29. Abou-Elfath, H. "Evaluating the ductility characteristics of self-centering buckling-restrained shape memory alloy braces", *Smart Materials and Structures*, **26**(5), p. 055020 (2017).

30. Andrawes, B. and Shin, M. "Seismic retrofitting of bridge columns using shape memory alloys", *Active and Passive Smart Structures and Integrated Systems*, p. 69281K (2008).

31. Rojob, H. and El-Hacha, R. "Self-prestressing using iron-based shape memory alloy for flexural strengthening of reinforced concrete beams", *ACI Structural Journal*, **114**(2), p. 523 (2017).

32. Izadi, M., Ghafoori, E., Shahverdi, M., Motavalli, M., and Maalek, S. "Development of an iron-based shape memory alloy (Fe-SMA) strengthening system for steel plates", *Engineering Structures*, **174**, pp. 433–446 (2018).

33. Vian, D., Bruneau, M., and Purba, R. "Special perforated steel plate shear walls with reduced beam section anchor beams. II: Analysis and design recommendations", *Journal of Structural Engineering*, **135**(3), pp. 221–228 (2009).

34. Kaufmann, E.J., Metrovich, B., and Pense, A.W. "Characterization of cyclic inelastic strain behavior on properties of A572 Gr. 50 and A913 Gr. 50 rolled sections", *National Center for Engineering Research on Advanced Technology for Large Structural Systems*, Lehigh University, Bethlehem, Pennsylvania (2001).

35. Wang, W., Chan, T.-M., Shao, H., and Chen, Y. "Cyclic behavior of connections equipped with NiTi shape memory alloy and steel tendons between H–shaped beam to CHS column", *Engineering Structures*, **88**, pp. 37–50 (2015).

36. Oliveira, J.P., Miranda, R.M., and Braz Fernandes, F.M. "Welding and joining of niti shape memory alloys: A review", *Progress in Materials Science*, **88**, pp. 412–466 (2017).

37. Chandler, A., Pappin, J., and Coburn, A. "Vulnerability and seismic risk assessment of buildings following the 1989 Newcastle, Australia earthquake", *Bulletin of the New Zealand National Society for Earthquake Engineering*, **24**(2), pp. 116–138 (1991).

38. Gholizadeh, S. and Salajegheh, E. "Optimal seismic design of steel structures by an efficient soft computing based algorithm", *Journal of Constructional Steel Research*, **66**(1), pp. 85–95 (2010).

39. Mohebbi, M., Shakeri, K., Ghanbarpour, Y., and Majzoub, H. "Designing optimal multiple tuned mass dampers using genetic algorithms (GAs) for mitigating the seismic response of structures", *Journal of Vibration Control*, **19**(4), pp. 605–625 (2013).

40. Kanai, K. "An empirical formula for the spectrum of strong earthquake motions", *Bulletin of the Earthquake Research Institute*, **39**, pp. 85–95 (1961).

41. Tajimi, H. "A statistical method of determing the maximum response of a building structure during an earthquake", In *Proc. 2nd World Conference on Earthquake Engineering*, pp. 781–797 (1960).

42. Wu, J., Chen, G., and Lou, M. "Seismic effectiveness of tuned mass dampers considering soil-structure interaction", *Journal of Earthquake Engineering and Structural Dynamics*, **28**(11), pp. 1219–1233 (1999).

Biographies

Reza Kamgar obtained his MS and PhD degrees in Civil Engineering from the Department of Civil Engineering at Shahid Bahonar University of Kerman, Kerman, Iran. He graduated in 2015 with top ranking and, at present, is a faculty member of Shahrekord University, Iran. His research interests include dynamics of structures, earthquake engineering, finite element method, ductile design of steel structures, vibration control, tall buildings, soil-structure interaction, structural optimization, constitutive model, and soft computing methods. He has published 110 journal and conference papers, and also six books.

Heisam Heidarzadeh obtained his PhD and MS degrees in Geotechnical Engineering from Tarbiat Modares University and the University of Tehran, respectively, and is currently Assistant Professor at Shahrekord University, Iran. His publications are mostly focused on the constitutive model, numerical methods and simulations, optimization, and dynamic analyses. He is considered an expert in these fields and cooperates with several journals as a reviewer.

Mohammad Reza Babadaei Samani obtained his MS degree in Civil Engineering in 2017 and is currently a researcher. He has published some journal and conference papers. His research areas of interest include earthquake engineering, structural optimization, and dynamics of structures.